Numerical models of P–T, time and grain-size controls on Ar diffusion in biotite: an aide to interpreting $^{40}Ar/^{39}Ar$ ages

Numerical models of P–T, time and grain-size controls on Ar diffusion in biotite: an aide to interpreting $^{40}Ar/^{39}Ar$ ages

D.R. Skipton[a*], C.J. Warren[b], F. Hanke[c]

[a]*Geological Survey of Canada, Natural Resources Canada, Ottawa, Ontario, K1A 0E8, Canada*

[b]*School of Environment, Earth and Ecosystem Sciences, The Open University, Walton Hall, Milton Keynes, MK7 6AA, United Kingdom*

[c]*Dassault Systèmes BIOVIA, 334 Science Park, Cambridge, CB4 0WN, United Kingdom*

*corresponding author: diane.skipton@canada.ca

Abstract

Dating of biotite using the $^{40}Ar/^{39}Ar$ method is used extensively to determine the timing of cooling and exhumation in metamorphic rocks. Interpretations of $^{40}Ar/^{39}Ar$ dates commonly assume that ^{40}Ar diffuses out of biotite through temperature-dependent volume diffusion, and therefore that the date represents the time at which biotite cooled through a closure temperature. Several processes, however, may perturb Ar systematics such that the $^{40}Ar/^{39}Ar$ date does not uniquely represent the timing of cooling through a closure temperature, including incomplete re-setting of Ar systematics, incorporation of excess Ar, crystal defects acting as Ar traps or fast-pathways, or fluid-present recrystallization/dissolution. We present a series of numerical diffusion model results that show the percentage of radiogenic Ar that should theoretically be retained in biotite with different grain radii residing for various periods over a range of P–T conditions, in a perfect open system that loses Ar via volume diffusion alone. A second set of models demonstrates the effects of different cooling rates on biotite $^{40}Ar/^{39}Ar$ dates and intra-grain Ar distributions in a perfect open system. The model results are useful for constraining cooling and exhumation histories from $^{40}Ar/^{39}Ar$ biotite data in a variety of metamorphic

settings. They also provide baseline data for biotite ^{40}Ar retention, $^{40}Ar/^{39}Ar$ ages and intra-grain age distributions that would theoretically be produced from volume diffusion acting alone. Consequently, the models can help evaluate the plausibility of alternative scenarios that may have affected biotite $^{40}Ar/^{39}Ar$ dates, including extraneous Ar contamination or Ar loss via processes other than diffusion. In conjunction with well-constrained petrogenetic histories, numerical diffusion models are a powerful tool for interpreting $^{40}Ar/^{39}Ar$ biotite ages, especially when linked with intra-grain $^{40}Ar/^{39}Ar$ age profiles.

Keywords

$^{40}Ar/^{39}Ar$ thermochronology, biotite, diffusion, numerical model, pressure-temperature, crustal residence

1. Introduction

Radioactive decay of ^{40}K produces ^{40}Ar, which has been shown to diffuse in biotite at temperatures above ~300°C in a direction parallel to cleavage over length scales comparable to mineral grain dimensions (e.g., 0.15 mm; Harrison et al., 1985). It is assumed that Ar strongly partitions from minerals into the grain boundary (fluid-bearing) network, consistent with open-system behaviour (e.g., Kelley, 2002). Therefore, $^{40}Ar/^{39}Ar$ dates yielded by metamorphic biotite are typically assumed to relate to temperature-dependent diffusional Ar loss and thus constrain the timing of cooling following metamorphism. The dating of biotite using the $^{40}Ar/^{39}Ar$ technique has been used for decades to constrain the timing of cooling, exhumation and low-temperature geological events worldwide (e.g., Berger, 1975; Hanson et al., 1975; Steltenpohl et al., 1993; Hodges and Bowring, 1995; McDougall and Harrison, 1999; Schneider et al., 1999, 2013; Willigers et al., 2001). For detailed discussion and calculations of Ar diffusion in biotite

and the closure temperature concept, we refer the reader to previous studies (Dodson, 1973, 1986; Harrison et al., 1985; Wheeler, 1996; McDougall and Harrison, 1999).

Several studies have identified complexities of ^{40}Ar concentrations in biotite that call into question traditional interpretations of metamorphic $^{40}Ar/^{39}Ar$ dates as resulting solely from temperature-controlled volume diffusion (Heizler and Harrison, 1988; Lee, 1995; Kelley, 2002; Villa, 2010; Warren et al., 2011; Camacho et al., 2012; Cossette et al., 2015; Mottram et al., 2015; Stübner et al., 2017). These studies suggest that alternative processes or scenarios affected the ^{40}Ar concentrations in biotite. Dates yielded by the $^{40}Ar/^{39}Ar$ method that are older than the timing of cooling through the closure temperature of ^{40}Ar ($T_c \approx$ 280-345°C; Harrison et al., 1985; McDougall and Harrison, 1999) can be produced by: (i) incomplete re-setting of mica during metamorphism, resulting in retention of "inherited" (pre-thermal peak) ^{40}Ar (Warren et al., 2012a; Mottram et al., 2015); (ii) incorporation and retention of excess Ar ($^{40}Ar_e$), which refers to parentless ^{40}Ar that is incorporated in the grain via diffusion from an Ar-rich grain boundary fluid network or contained within mineral/fluid inclusions (Kelley, 2002); (iii) planar defects in the crystal structure serving as ^{40}Ar traps (proposed in trioctohedral mica; Camacho et al., 2012); or (iv) recrystallization in a closed Ar-rich system, adding ^{40}Ar to grain rims (Warren et al., 2011). Dates yielded by the $^{40}Ar/^{39}Ar$ technique that are younger than the age of cooling through T_c can result from: (i) crystallization of the grain at or below T_c (e.g., Warren et al. 2012); (ii) planar defects in the crystal structure, such as those produced during deformation, serving as fast-pathways through which ^{40}Ar can escape (Lee, 1995; Hodges and Bowring, 1995; Cosca et al., 2011); and (iii) isotopic resetting (^{40}Ar loss) due to fluid-present retrograde reactions / recrystallization / dissolution (Villa, 2010).

Metamorphic biotite is infamous for yielding $^{40}Ar/^{39}Ar$ dates that are older than those expected from volume diffusion during residence at high temperatures or cooling through the estimated Ar T_c. Despite the higher Ar T_c for muscovite (~420–450°C; Harrison et al., 2009), biotite in some cases yields $^{40}Ar/^{39}Ar$ dates that are substantially older than those of muscovite from the same rock, and may also pre-date U/Pb ages of metamorphic monazite or zircon. Such age relationships have been documented in several orogens, including the Paleoproterozoic Trans-Hudson (Skipton et al., 2017), Mesoproterozoic Grenville (Dallmeyer and Rivers, 1983; Cosca et al., 1991; Smith et al., 1994), Neoproterozoic Capricorn (Occhipinti and Reddy, 2009), Mesozoic Alpine (Brewer, 1969; Pickles et al., 1997) and Himalayan orogens (Mottram et al., 2015; Stübner et al., 2017).

In the event that biotite yields a $^{40}Ar/^{39}Ar$ date that defies independent geological or isotopic evidence, the anomalous $^{40}Ar/^{39}Ar$ ratio is typically attributed to processes other than (or in addition to) volume diffusion, involving inherited or excess ^{40}Ar, crystal defects, recrystallization, dissolution, as described above, or dehydroxylation during vacuum heating (Foland, 1983; Harrison et al., 1985; Gaber et al., 1988; McDougall and Harrison, 1999). The degree of potential interpretational inaccuracy in such biotite ages is difficult to quantify, especially without models of Ar retention for different biotite radii and P–T histories. This has resulted in non-uniform interpretations of biotite $^{40}Ar/^{39}Ar$ data – which may be arbitrary without conclusive evidence for the process being invoked – and a general distrust and avoidance of biotite $^{40}Ar/^{39}Ar$ dating in recent metamorphic studies.

Here we present numerical models for volume diffusive loss of ^{40}Ar out of biotite over a range of geologically relevant temperatures (200–650°C) and pressures (0–2 GPa), and for different grain radii (0.1–5 mm) and residence times (1–1000 Myr). These models provide a

93 baseline for ideal ^{40}Ar diffusion behaviour in biotite, according to experimentally established
94 diffusion parameters, and demonstrate theoretical ^{40}Ar retentivity for various P–T scenarios to
95 help interpret cooling/exhumation histories. Our models also enable comparisons with equivalent
96 models for muscovite (Warren et al., 2012a) to aid age interpretations in cases of co-existing
97 biotite and muscovite. By calculating percentages of ^{40}Ar retention in biotite that would be
98 expected from volume diffusion acting alone, the models provide constraints on whether or not
99 alternative processes may have affected the sample ^{40}Ar/^{39}Ar date. The models illustrate the
100 significance of grain size, P–T and crustal residence time on ^{40}Ar diffusion, and demonstrate that
101 extraneous Ar or changes to mica structure do not necessarily have to be invoked to explain
102 ^{40}Ar/^{39}Ar dates that seem to conflict with other geochronometers. Our models also help to rule-in
103 or rule-out certain scenarios, such as whether or not a ^{40}Ar/^{39}Ar result could reflect the timing of
104 biotite growth, or the retention of pre-thermal peak radiogenic ^{40}Ar. Argon loss via dissolution-
105 recrystallization would be faster than via diffusion, and assessing Ar retention as a function of
106 temperature in biotite affected by dissolution-recrystallization would be invalid (Villa, 2010).
107 Our models still apply in these cases, but only if the initial ("starting") temperature of the model
108 is taken to be the temperature of recrystallization.

109

110 **2. Methodology: numerical modeling of ^{40}Ar diffusion in biotite**

111 Numerical models of ^{40}Ar diffusion in biotite were run using the program DiffArgP
112 (Wheeler, 1996; Warren et al., 2012a) in GNU Octave. The following parameters were used for
113 the models (excluding uncertainties): activation energy (E_a) = 47 ± 2 kcal mol^{-1} (196 648 J mol^{-1};
114 Harrison et al., 1985); diffusion coefficient (D_0) = 0.077 $^{+0.21}_{-0.06}$ cm^2 s^{-1} (Harrison et al., 1985); and

activation volume (V_{act}) = 14 cm^3 mol^{-1} (Harrison et al., 1985; Grove and Harrison, 1996; Harrison et al., 2009).

The models were run using a cylindrical geometry because diffusive Ar loss in mica mainly occurs through cleavage-parallel diffusion in the crystal, which is typically modeled using cylindrical symmetry (Giletti, 1974; Giletti and Tullis, 1977). There has been some debate about the geometry used to model these systems, but detailed analysis of diffusion coefficients has shown that the symmetry effects (e.g. cylindrical vs. spherical) on diffusion coefficients (refer to Forster and Lister, 2014) are substantially smaller than the uncertainties on the measured diffusion parameters listed above. A Crank-Nicholson solver was used for the time integration with a time step that is 10 times larger than that required for the fully explicit model (Wheeler, 1996; Warren et al., 2012a). It was assumed that volume diffusion occurred in an open system where the Ar concentration at the grain boundary was negligible (i.e., no $^{40}Ar_e$ in the grain boundary network) and the grain radius was equivalent to the diffusion radius. To achieve full numerical precision on the model ages, we ran each model at four different mesh lengths and then plotted the four integrated, or "bulk", ages against mesh spacing (grain radius/mesh length). These data define a linear function for which the intercept of the regression line at zero mesh spacing yields the bulk age of the model with an infinitely dense integration mesh, and, therefore, with the highest numerical precision possible (Warren et al., 2012a, 2012b). Representative model output data (bulk $^{40}Ar/^{39}Ar$ age and core-to-rim $^{40}Ar/^{39}Ar$ age profile) and bulk age linear regression plots are shown in Supplementary File 1.

Models were run for a range of biotite grain radii (0.1, 0.5, 1, 2 and 5 mm) that are representative of the grain sizes typically analyzed for $^{40}Ar/^{39}Ar$ thermochronology. The models simulated crustal residence times of 1, 5 and 20 Myr, characteristic residence timescales for

138 metamorphism in both modern and ancient orogens (e.g., 1–10 Myr, ca. 470 Ma Grampian
139 Orogen, Scotland, Viete et al., 2011; 20–40 Myr, ca. 1830 Ma Trans-Hudson Orogen, Canada,
140 Skipton et al., 2016; ≤1–5 Myr, ca. 21–10.5 Ma Sikkim Himalaya, Mottram et al., 2015).
141 Residence times of 100, 500 and 1000 Myr were also modeled for grain radii of 0.1 to 1 mm to
142 illustrate how Ar retention might be affected by long-term crustal residence, which is likely in
143 Precambrian orogens. For a given biotite grain radius and residence time, models were run for a
144 range of temperatures at 10°C increments to cover the full spectrum of Ar retention from 0%
145 (complete ^{40}Ar loss) to 100% (all ^{40}Ar retained). Models were run using a pressure of 0.5 GPa;
146 Ar retention at different pressures (0–2 GPa) was calculated using established values of E_a, P_0
147 and V_{act} (above) to map out equivalent diffusion coefficients across the entire pressure range.
148 These model results were used to construct P–T diagrams showing %Ar retention in biotite for
149 temperatures of 200–650°C and pressures up to 2 GPa (Figs. 1–3).

150 A second set of models was run to simulate the effects of various cooling/exhumation
151 histories on Ar retention in a biotite grain with a 0.5 mm radius (Figs. 4–6). For these models,
152 biotite was first maintained at a temperature of 250°C, 350°C or 450°C and pressure of 0.7 GPa
153 for different residence times (1, 20, 100, 500 or 1000 Myr). These conditions correspond to the
154 red, blue and intermediate zones in the P-T-% retention plots in Figs. 1–3. Following the defined
155 residence periods, the modeled biotite was cooled at rates of 1.5, 10 or 30°C/Myr, which are
156 representative of cooling rates documented/suggested in Proterozoic and modern orogens (e.g.,
157 Dunlap, 2000). Decompression was modelled linearly with cooling, such that 0°C and 0 GPa
158 were attained simultaneously in each model. A start time of 1500 Ma was used for this set of
159 models to present all the modeled residence periods, temperatures and cooling rates from a
160 common point in time, enabling straightforward comparison between models results shown in

Figs. 4–6. The start time is otherwise arbitrary. The key detail is the amount of time that went unrecorded in the mica due to low Ar retention, i.e., the difference between the time at which the model started and the bulk age calculated by DiffArgP. In effect, the models can be applied to any period of geological interest.

3. Model results

3.1. Plots of pressure–temperature–%Ar retention

Model results are shown on pressure–temperature plots with colour shading corresponding to percentages of ^{40}Ar retention (Figs. 1–3). As with equivalent models constructed for muscovite (Warren et al., 2012a), the blue zones represent P–T conditions of low Ar retention, the red zones represent conditions of high Ar retention, and orange-to-light blue zones reflect conditions of intermediate or partial Ar retention.

The plots illustrate the significant dependence of ^{40}Ar retention in biotite on grain size and residence time, even for relatively short residence times of 1–20 Myr (Figs. 1, 2). For a given set of crustal residence conditions (temperature, pressure, time) within the intermediate zone, biotite with a 0.1 mm radius (Fig. 2d-f) is ~35% less retentive of Ar than biotite with a 1 mm radius (Fig. 1g-i), which is ~25% less retentive than biotite with a 5 mm radius (Fig. 1a-c). For a biotite grain with a given radius residing at fixed P–T conditions in the intermediate zone, a grain residing for 20 Myr (Figs. 1c, f, i; 2c, f) is ~35% less retentive than biotite residing for 1 Myr (Figs. 1a, d, g; 2a, d).

The plots simulating long-term crustal residence of 100–1000 Myr demonstrate the effects of geologic time on ^{40}Ar concentrations in biotite, especially in Precambrian orogens (Fig. 3). For a 1 mm-radius biotite residing for 20 Myr at set P-T conditions within the partial Ar

retention zone (Fig. 1i), Ar retention is ~20, 40 or 60% lower for residence times of 100, 500 or 1000 Myr, respectively (Fig. 3a-c). Time exerts the most extreme effects on Ar systematics in fine-grained, 0.1 mm-radius biotite: during 1 Gyr residence at upper-crustal conditions of 250°C ($<T_c$) and $P \leq 0.5$ GPa, models suggest that the grain would lose at least ~50% radiogenic Ar through diffusion (Fig. 3i) before exhumation starts.

3.2. Models of cooling and exhumation histories for biotite with a 0.5 mm radius

Model results are shown as core-to-rim $^{40}Ar/^{39}Ar$ age profiles with corresponding bulk ages, calculated using a model start time of 1500 Ma (Figs. 4–6). For models in which biotite resided at 250°C for 1–100 Myr prior to cooling, bulk ages are ≤1 Myr younger than the onset of crustal residence (i.e., the model start time), and core-to-rim age profiles are relatively flat regardless of cooling rate (Figs. 4a–b, 5a). For residence times of 500 Myr and 1 Gyr at 250°C, however, modelled core-to-rim age profiles exhibit diffusive Ar loss at outer grain edges and yield bulk ages that are 28–30 Myr and 81–84 Myr, respectively, younger than the onset of crustal residence (Figs. 5b, 6a).

For models in which biotite crystallised and resided at relatively cool temperatures of 350°C for various periods prior to cooling, slower cooling rates produce younger bulk ages and greater core-to-rim age decreases than those produced by faster cooling rates. For a residence time of 1 Myr at 350°C, model ages are up to 10 Myr younger than the onset of cooling below 350°C in each model (Fig. 4c). However, for all other residence periods modeled (20 Myr to 1 Gyr; Figs. 4d, 5d, 6b), resultant ages are older than the onset of cooling or, in the case of cooling at 1.5°C after 20 Myr residence (Fig. 4d), only 4 Myr younger than the onset of cooling.

Models of biotite crystallising then residing at higher temperatures (e.g., 450°C) for various periods followed by cooling at different rates all yielded ages younger than the onset of cooling (Fig. 4e, f; 5e, f; 6c). The slower the cooling rate, the younger the bulk age and the steeper the core-to-rim age profile, with all ages younger than those of equivalent models run with 350°C residence conditions. Notably, for residence periods of 20 Myr and longer, core-to-rim age profile slopes of the 350°C models are steeper than those of 450°C models with equivalent cooling rates.

4. Discussion

4.1. Applicability of experimentally-determined Ar diffusion parameters to natural samples

Few studies have successfully conducted experimental measurements of ^{40}Ar diffusivity in biotite, in part due to the difficulty of maintaining the stability of hydroxyl-bearing minerals over the necessary temperature range. Harrison et al. (1985) addressed this issue by measuring radiogenic ^{40}Ar loss from biotite samples after hydrothermal-isothermal treatment; for each temperature run, biotite was heated at constant temperature in the presence of water to help maintain the mineral's stability. The biotite samples were ~56% annite, with radii of 56–202 μm, typical of biotite in granite and in most metamorphic rocks dated using ^{40}Ar/^{39}Ar (e.g., meta-granite, pelite, psammite). Equivalent experiments conducted on Fe-rich biotite provided nearly identical diffusion parameters (Grove and Harrison, 1996). For these reasons, in the absence of other reliable experimental values, and to be consistent with most interpretations of ^{40}Ar/^{39}Ar biotite data we used the E_a and D_0 of Harrison et al. (1985) here (a comprehensive review is provided by McDougall and Harrison, 1999).

It has been argued that lab-measured diffusivities of hydrous minerals (biotite, phlogopite, muscovite) are too high compared to those affecting natural resetting of geochronometers due to greater artificially-induced ^{40}Ar loss during heating experiments (Villa, 1994, 2010). During initial heating, insufficient water activity in the experimental capsule leads to dehydroxylation, whereas excessive water activity can result in aqueous dissolution. Both processes may create pathways through which ^{40}Ar can escape more rapidly than in nature, resulting in overestimation of the measured volume diffusivities (Villa, 2010). Corrected activation energies and diffusion coefficients have been estimated for phlogopite (Villa, 2010), however, correction factors are based on an assumed percentage (~6%) of initial fast-pathway ^{40}Ar loss required to fit lines through measured data. As such, the amount of fast-pathway ^{40}Ar loss from biotite during diffusion experiments is not reliably quantifiable, and corrections for fast-pathway ^{40}Ar loss in experimentally determined E_a and D_0 are not built into our models. This may represent a source of uncertainty in the calculated percentages of ^{40}Ar retention, such that biotite may retain more ^{40}Ar in reality than the modeled percentages. Nonetheless, ^{40}Ar/^{39}Ar mica dates have, in many settings, been documented to align with those predicted by measured Ar diffusivities and other isotopic systems (i.e., the ^{40}Ar/^{39}Ar age of biotite < muscovite < hornblende < U/Pb ages; e.g., Van Schmus et al., 2007; Schneider et al., 2013; Willigers et al., 2001), suggesting that the measured diffusivities are likely close to those operating in nature.

Uncertainties on experimentally determined diffusion parameters must also be taken into account. Inclusion of the uncertainties on D_0 and E_a (Harrison et al., 1985) in our models corresponds to uncertainty of up to ±50°C on the temperature associated with any given percentage of ^{40}Ar retention (Figs. 1–3). This margin of error is not much more significant than the ±0.5 kbar and ±25°C uncertainties suggested for P–T estimates (Powell and Holland, 2008),

which are used to determine the metamorphic conditions experienced by the dated biotite and, therefore, where the biotite plots in P–T space in Figures 1–3.

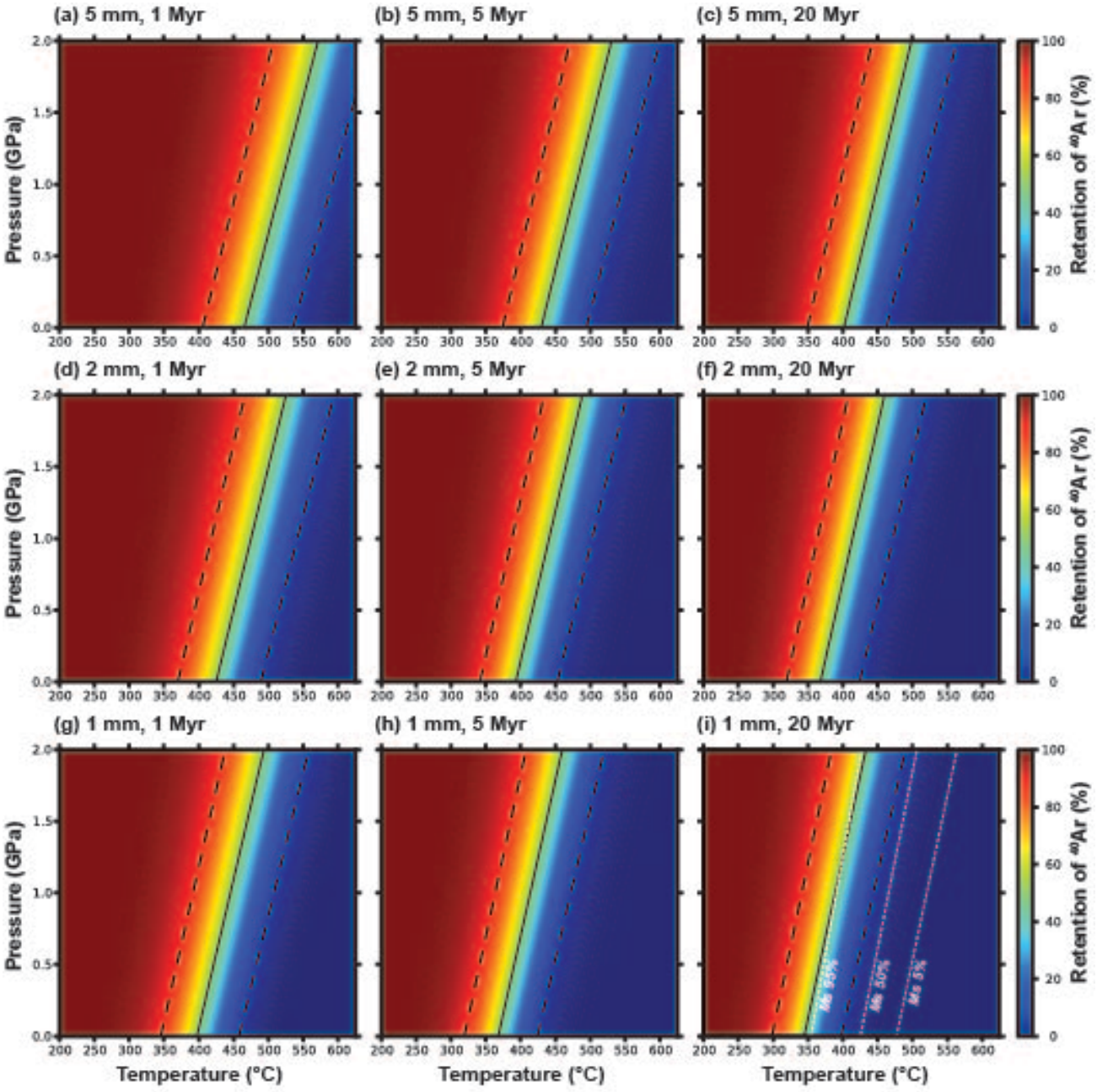

Figure 1

Fig. 1: *Pressure–temperature diagrams colour coded with percentages of radiogenic Ar retained in biotite, as calculated from numerical diffusion models for biotite grains with radii of 1, 2 and 5 mm residing at the given P–T conditions for periods of 1, 5 and 20 Myr. White dashed lines indicate percentages of radiogenic Ar retained in muscovite, modelled by Warren et al. (2012a). The 50% retention contour is indicated with a black solid line. Black dashed lines show the limits of diffusion parameter uncertainties on the 50% retention contour.*

Nonetheless, it is significant enough that diffusion parameter uncertainties are important to consider when using these plots as an aide for interpreting biotite $^{40}Ar/^{39}Ar$ dates. Furthermore, the numerical values of ^{40}Ar retention calculated from our models are highly dependent on the measured diffusion parameters for biotite, as well as their uncertainties. If future experiments succeed in keeping biotite stable during heating, and new measured diffusion parameters are deemed more accurate than those of Harrison et al. (1985), our models would need to be updated with the new parameters. Although the use of different diffusion parameters, and/or the application of uncertainties, would change the calculated percentages of ^{40}Ar retention in Figures 1-3, the main concepts shown by our models remain unaffected. The models show how the metamorphic evolution and grain size will affect Ar retention in biotite: every biotite grain has a P–T region for which it would retain most, if not all of its radiogenic ^{40}Ar. As this P–T region covers broader temperatures at higher pressures, a $^{40}Ar/^{39}Ar$ date from biotite with a low-temperature / high-pressure history may not represent a cooling age. This point remains valid for any set of diffusion parameters (D_0, E_a, V_0).

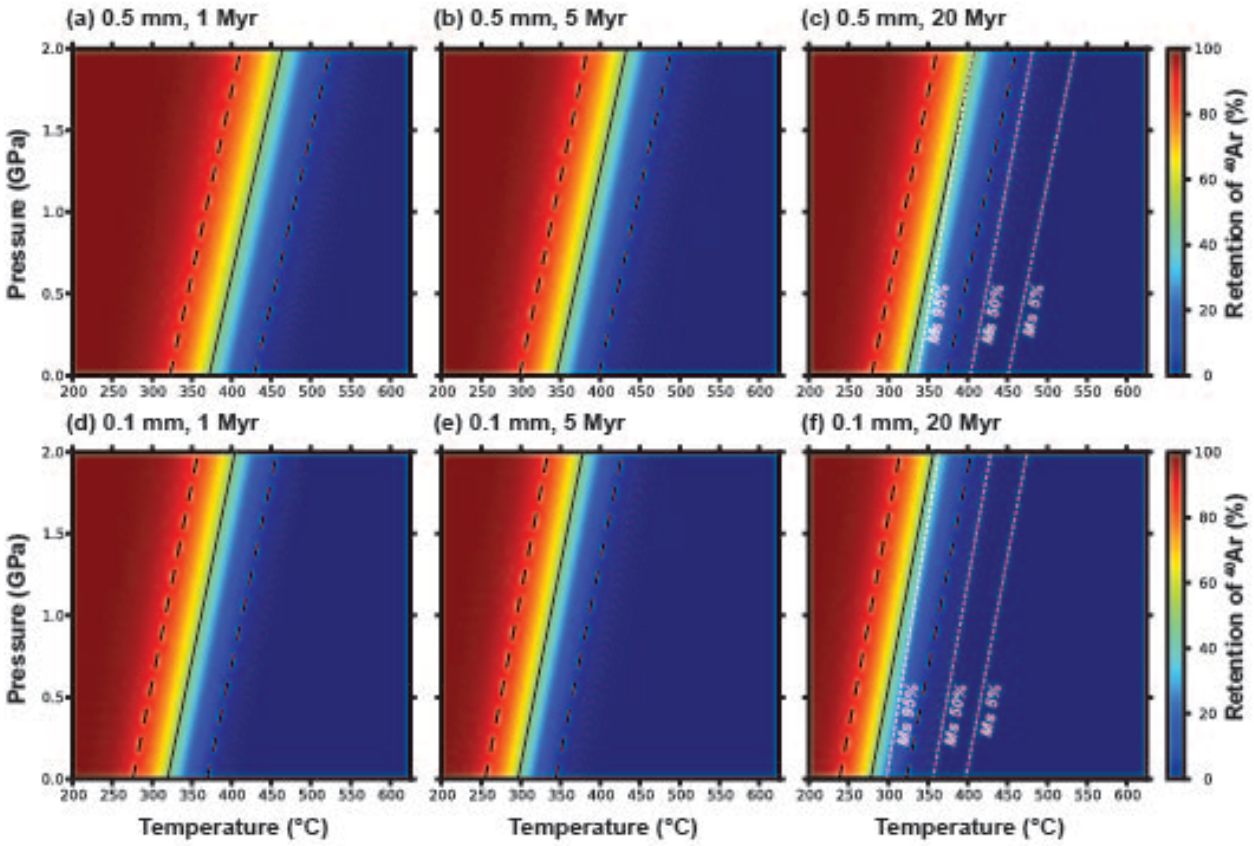

Figure 2

Fig. 2: *Pressure–temperature diagrams colour coded with percentages of radiogenic Ar retained in biotite, as calculated from numerical diffusion models for biotite grains with radii of 0.5 and 0.1 mm residing at the given P–T conditions for periods of 1, 5 and 20 Myr. White dashed lines indicate percentages of radiogenic Ar retained in muscovite, modelled by Warren et al. (2012a). The 50% retention contour is indicated with a black solid line. Black dashed lines show the limits of diffusion parameter uncertainties on the 50% retention contour.*

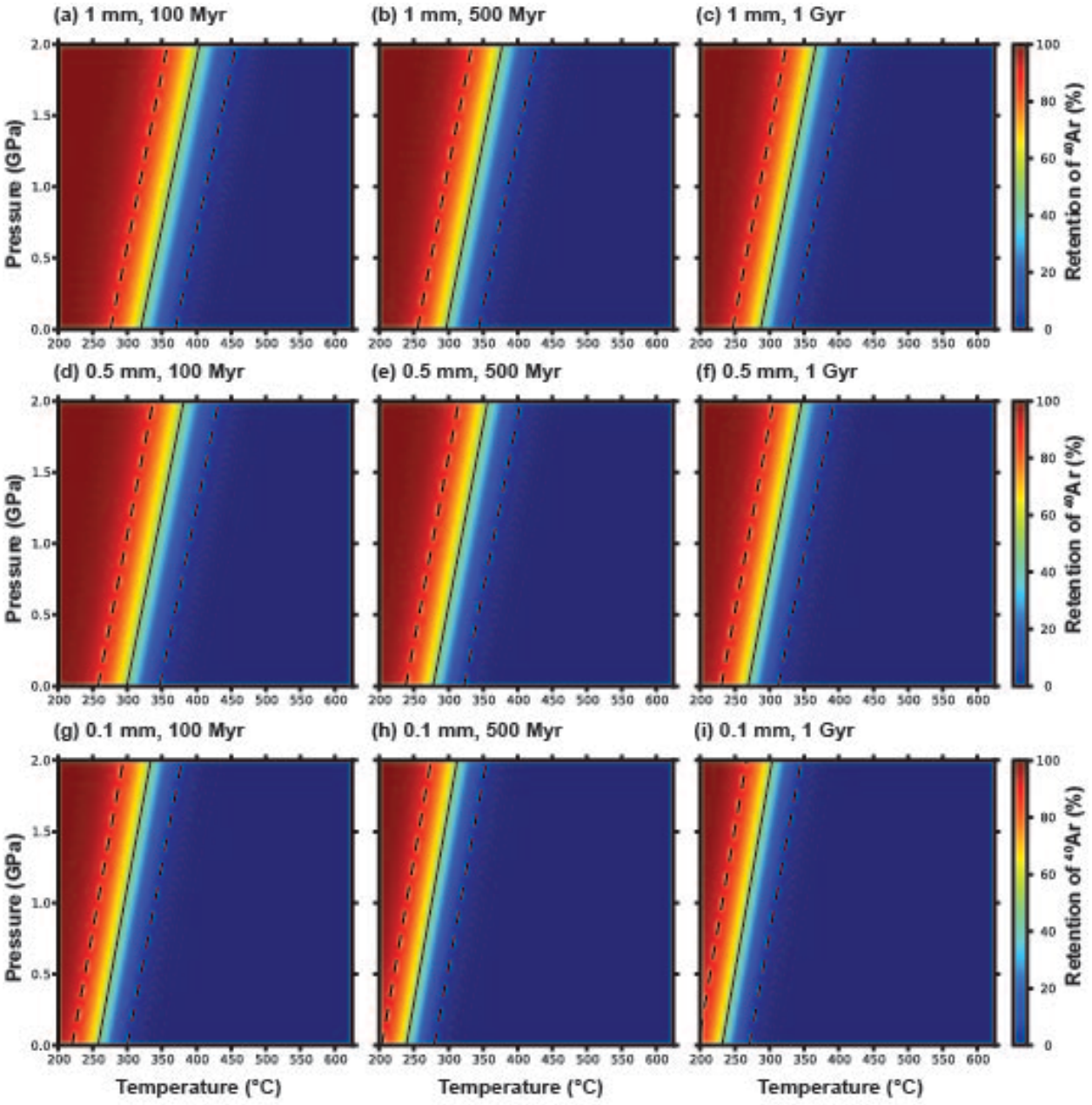

Figure 3

Fig. 3: *Pressure–temperature diagrams colour coded with percentages of radiogenic Ar retained in biotite, as calculated from numerical diffusion models for biotite grains with radii of 1, 0.5 and 0.1 mm residing at the given P–T conditions for periods of 100 Myr, 500 Myr and 1 Gyr.*

289 *The 50% retention contour is indicated with a black solid line. Black dashed lines show the*
290 *limits of diffusion parameter uncertainties on the 50% retention contour.*
291

292 **4.2. Model interpretation**

293 The modeled P-T-% retention plots (Figs. 1-3) show that biotite that crystallized in or
294 experienced peak metamorphism in P–T zones of low Ar retention (blue zones in Figs. 1-3)
295 would not theoretically retain any pre-thermal peak (inherited) radiogenic Ar. It should therefore
296 record the timing of its cooling and exhumation. Due to high Ar retention in the red P–T zones,
297 the $^{40}Ar/^{39}Ar$ date of biotite that crystallized at these conditions should, in an ideal system, reflect
298 the timing of its crystallization. Biotite that crystallised at lower conditions and subsequently
299 experienced peak metamorphism in the red P–T zones would not lose its inherited (pre-thermal
300 peak) ^{40}Ar before cooling initiated. Even if such a grain lost some Ar during cooling, it would
301 still yield an older $^{40}Ar/^{39}Ar$ date than a grain that had crystallised at peak conditions, potentially
302 resulting in overestimation of interpreted cooling rates. A $^{40}Ar/^{39}Ar$ date of biotite that
303 crystallized in or experienced peak metamorphism in the intermediate (light blue to orange) P–T
304 zones must also be interpreted with caution due to incomplete pre-peak degassing of ^{40}Ar.

305 The results of modeling different cooling and exhumation histories for biotite with a 0.5 mm
306 radius (Figs. 4-6) show insignificant Ar diffusion in biotite that resided at 250°C for 1-100 Myr,
307 as expected so far below the estimated T_c window. This is indicated by bulk ages that are ≤1 Myr
308 younger than the onset of crustal residence, and consistently flat core-to-rim age profiles
309 regardless of cooling rate (Figs. 4a–b, 5a). However, models of biotite grains with residence
310 times of 500 Myr and 1 Gyr at 250°C exhibit diffusive Ar loss at outer grain edges and yielded

311 bulk ages that are up to 84 Myr younger than the onset of crustal residence (Figs. 5b, 6a). This
312 implies that low-temperature Ar 'leakage' from the outermost ≤50 μm of grain edges may be
313 possible during long-term crustal residence of 0.5 mm-radius biotite in Precambrian orogens, and
314 may affect $^{40}Ar/^{39}Ar$ step-heating or total fusion dates beyond analytical uncertainty.

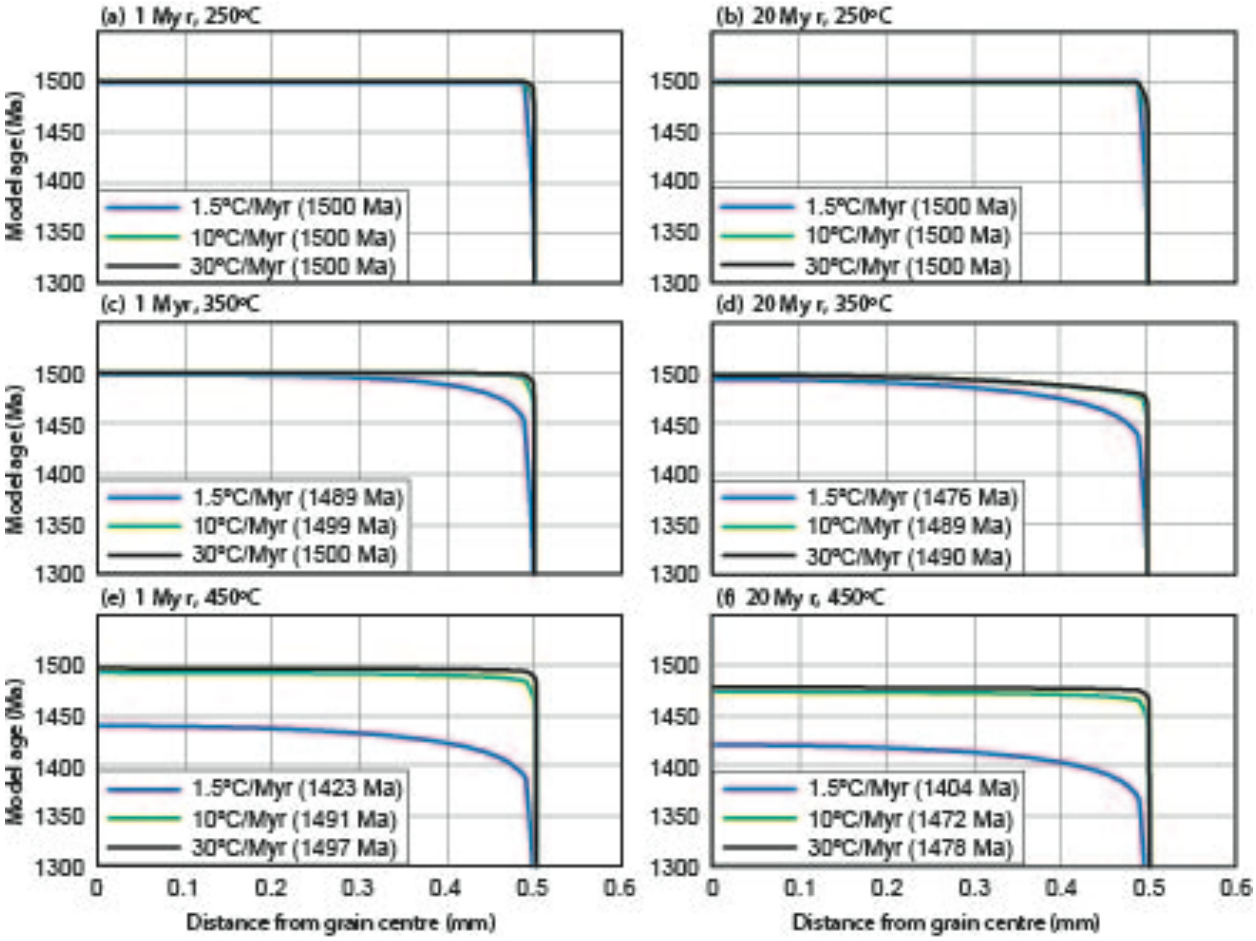

Figure 4

315 ***Fig. 4:*** *Modelled core-to-rim $^{40}Ar/^{39}Ar$ age profiles for 0.5 mm-radius biotite that remained at*
316 *temperatures of 250°C, 350°C or 450°C for 1 Myr or 20 Myr, then cooled at rates of 1.5°C/Myr,*
317 *10°C/Myr or 30°C/Myr. All models were run with an initial pressure of 0.7 GPa, followed by*
318 *decompression that occurred simultaneously with cooling. Models were run from an arbitrary*
319 *starting time of 1500 Ma (see text for details), such that the onset of cooling is 1499 Ma after a 1*

Myr residence period (a, c, e), and 1480 Ma following a 20 Myr residence period (b, d, f). Model bulk ages are shown in parentheses for each cooling rate.

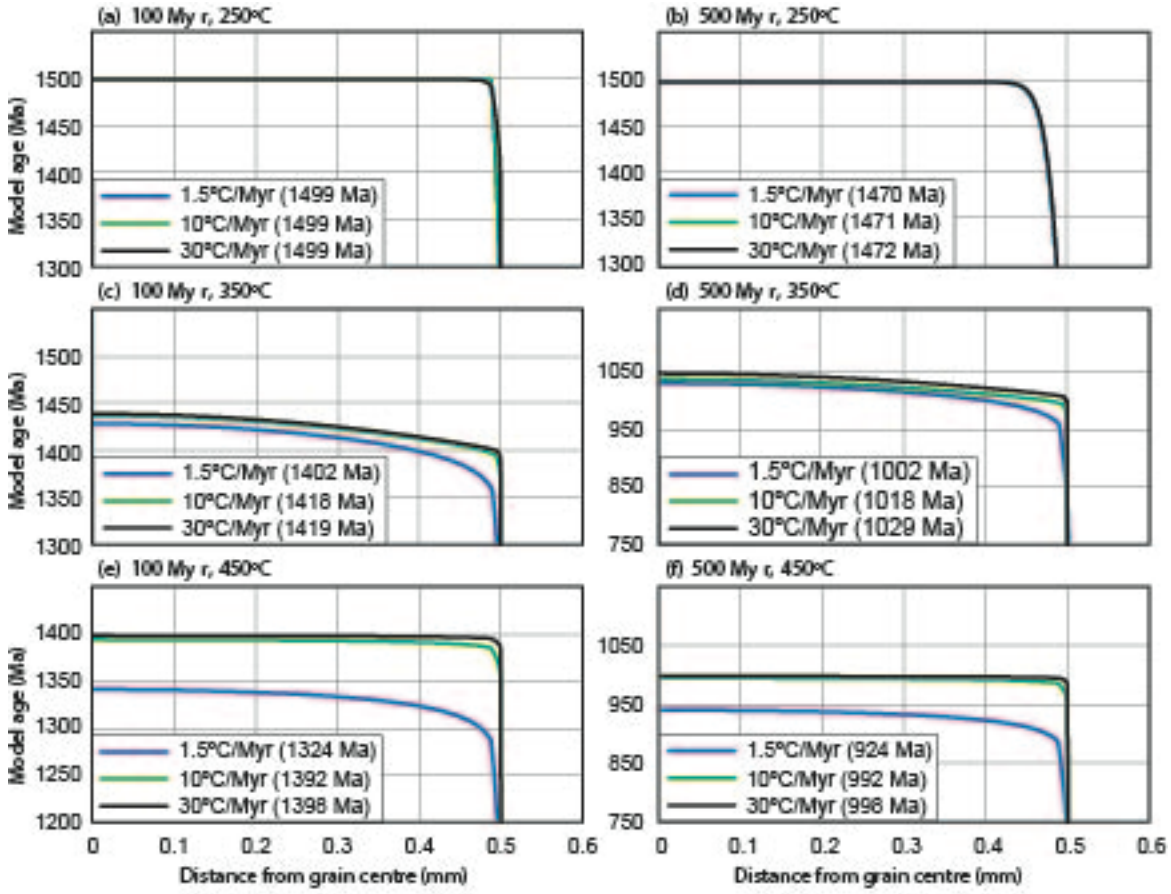

Figure 5

Fig. 5: *Modelled core-to-rim $^{40}Ar/^{39}Ar$ age profiles for 0.5 mm-radius biotite that remained at temperatures of 250°C, 350°C or 450°C for 100 Myr or 500 Myr, then cooled at rates of 1.5°C/Myr, 10°C/Myr or 30°C/Myr. All models were run with an initial pressure of 0.7 GPa, followed by decompression that occurred simultaneously with cooling. Models were run from an arbitrary starting time of 1500 Ma (see text for details), meaning that cooling began at 1400 Ma after a 100 Myr residence period (a, c, e) and at 1000 Ma following a 500 Myr residence period (b, d, f). Model bulk ages are shown in parentheses for each cooling rate.*

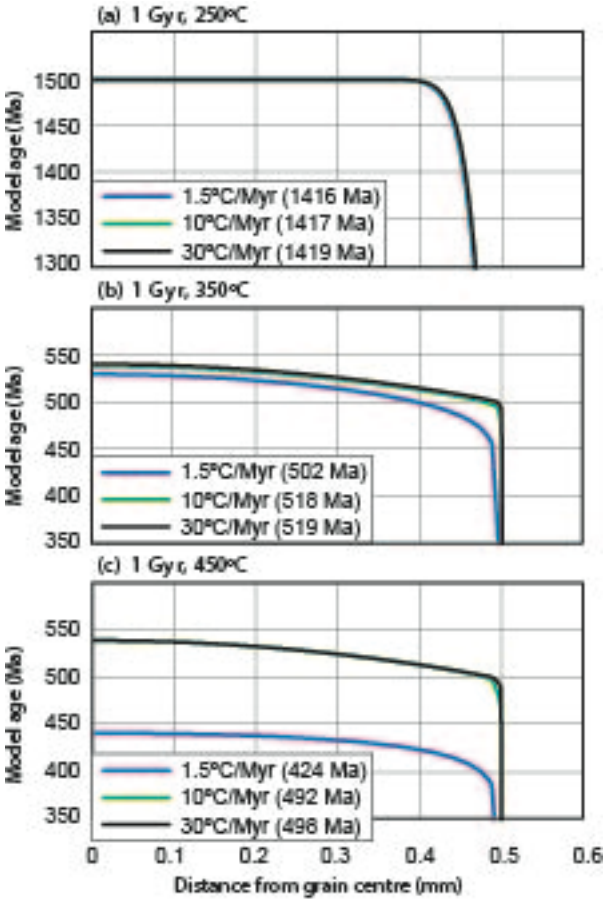

Figure 6

Fig. 6: *Modelled core-to-rim $^{40}Ar/^{39}Ar$ age profiles for 0.5 mm-radius biotite that remained at temperatures of 250°C, 350°C or 450°C for 1 Gyr, then cooled at rates of 1.5°C/Myr, 10°C/Myr or 30°C/Myr. All models were run with an initial pressure of 0.7 GPa, followed by decompression that occurred simultaneously with cooling. Models were run from an arbitrary starting time of 1500 Ma (see text for details), such that the onset of cooling occurred at 500 Ma. Model bulk ages are shown in parentheses for each cooling rate.*

For models in which biotite resided at 350°C prior to cooling, slowly cooled biotite grains produced younger bulk ages and greater core-to-rim age decreases than biotite that cooled more quickly. This relationship reflects relatively efficient Ar diffusion at 350°C, particularly for grains that remained hotter for longer and/or cooled more slowly. For most residence periods at 350°C (20 Myr to 1 Gyr; Figs. 4d, 5d, 6b), the modeled ages are older than the onset of cooling, which illustrates the possible partial retention of ^{40}Ar in biotite during residence within the 'intermediate' P–T zone, and the importance of knowing the P–T conditions of biotite growth as well as its subsequent P–T path for interpreting the measured $^{40}Ar/^{39}Ar$ date.

353 In accordance with highly efficient ^{40}Ar diffusion at 450°C, models of biotite crystallising
354 then residing at 450°C prior to cooling all yielded ages younger than the onset of cooling (Fig.
355 4e, f; 5e, f; 6c), regardless of residence time or cooling rate. The slower the cooling rate, the
356 younger the bulk age and the steeper the core-to-rim age profile, and the ages yielded by models
357 simulating residence at 450°C are younger than those of equivalent models run with 350°C
358 residence conditions. These relationships are consistent with sustained diffusion of ^{40}Ar out of
359 biotite that remains hotter than T_c for longer. The steeper slopes of the core-to-rim age profiles
360 for the 350°C models, relative to those of 450°C models with equivalent cooling rates, are
361 inferred to reflect the slower diffusion of Ar at 350°C, hindering transport of Ar from the grain
362 cores to the grain rims. Conversely, biotite residing at 450°C would experience more efficient Ar
363 loss, such that the core-to-rim age gradient is controlled solely by the subsequent cooling rate.
364 This is supported by our 450°C models: each cooling rate produced a distinct core-to-rim age
365 gradient that is unaffected by residence time or when cooling began.

366 **4.3. Interpreting exhumation and cooling**

367 By illustrating how Ar retention in biotite varies with pressure, temperature, grain size and
368 residence time, our modeled P–T–% retention plots can be used to help interpret cooling
369 histories from ^{40}Ar/^{39}Ar data in a variety of metamorphic regions. Our modeled ages and core-to-
370 rim age profiles of hypothetical cooling/exhumation scenarios may also inform tectonic
371 interpretations, especially when linked with spatially-controlled ^{40}Ar/^{39}Ar data, such as provided
372 by laser ablation.

373 Mica intra-grain age maps from UV laser spot analyses reveal abundant information, together
374 with step-heating or total-fusion ^{40}Ar/^{39}Ar data for comparison (e.g., Scaillet et al., 1990; de Jong
375 et al., 1992; Hodges and Bowring, 1995). Previous studies have matched measured core-to-rim

age profiles with diffusion model results to constrain cooling rates and cooling/exhumation histories (e.g., Hodges and Bowring, 1995; Kelley and Wartho, 2000; Wartho et al., 2003; Warren et al., 2011, 2012b; Skipton et al., 2017). Interpretations of cooling histories from UV laser age maps may be limited by the spatial resolution (at least 30–50 μm laser spot size usually required) and analytical errors of UV laser spot ages. Intra-grain age complexities and potential breakage of crystal edges during sample preparation (if analyzing mineral separates) present additional challenges, and the uncertainties inherent in DiffArgP modeling and biotite diffusion parameters (discussed above) necessitate caution when comparing $^{40}Ar/^{39}Ar$ dates with model results. Even so, we consider such comparisons to be the ideal approach for interpreting $^{40}Ar/^{39}Ar$ dates as related to cooling, crystallisation or $^{40}Ar_e$ contamination. Additionally, application of the $^{40}Ar/^{39}Ar$ single-grain total-fusion method to biotite to reveal grain-size controls on Ar distribution, in conjunction with diffusion models, may shed further light on the geological significance of ages, as has been shown for white mica (Mottram et al., 2015; Uunk et al., 2018).

4.3.1. High-grade metamorphism

The models suggest that biotite from medium- to high-grade rocks where the thermal peak is ≥600°C would have completely lost any pre-peak (inherited) radiogenic Ar, even if peak metamorphism lasted for only 1 Myr (Figs. 1g, 2a, 2d). Possible exceptions include coarse-grained biotite (2–5 mm radii) residing at pressures ≥1 GPa (Fig. 1a, d). Efficient Ar diffusion ≥600°C – even during short-lived thermal maxima – is supported by analyses of Himalayan biotite grains (0.25–0.5 mm radii) metamorphosed at ≥650°C for ~5 Myr, which yielded dates consistent with cooling ages (Mottram et al., 2015). Therefore, our results indicate that biotite that experienced amphibolite- to granulite-facies metamorphism is a candidate for yielding

399 $^{40}Ar/^{39}Ar$ cooling and exhumation ages, assuming an open grain boundary system. In this, our
400 models are in agreement with the long-held protocol for interpreting cooling ages from biotite in
401 high-grade metamorphic rocks.

402 *4.3.2. Low-grade and/or short-lived metamorphism*

403 Temperatures attained during peak greenschist or sub-greenschist-facies metamorphism
404 approach, or are lower than, previous estimates of closure temperatures of Ar in biotite ($T_c \approx$
405 280–345°C; Harrison et al., 1985; McDougall and Harrison, 1999). Biotite that crystallised along
406 the prograde path may therefore retain a percentage of pre-thermal peak ^{40}Ar (i.e., its Ar
407 systematics are not fully reset), and produce a $^{40}Ar/^{39}Ar$ date that is older than the predicted
408 cooling age had the biotite crystallised at, and cooled from, higher peak temperatures. Our
409 models provide graphical representation of this scenario, allowing a quantitative estimate of
410 whether or not inherited Ar could be a factor in biotite of a range of grain sizes residing at
411 various conditions. For example, a biotite grain with a 1 mm radius metamorphosed at 375°C (P
412 >0.5 GPa) would need to remain at those conditions for >20 Myr to lose its pre-peak Ar (Figs.
413 1g–i, 3a–c). If metamorphosed at 375°C for 20 Myr, a coarser-grained crystal (2–5 mm radius)
414 would retain at least ~50% inherited Ar, regardless of pressure (Fig. 1c, f). The models show that
415 biotite grains with smaller radii (~0.1–0.5 mm) are the safest choice for constraining the cooling
416 age following peak greenschist-facies metamorphism. Biotite grains that experienced thermal
417 peak at sub-greenschist-facies (≤300–350°C) are capable of yielding $^{40}Ar/^{39}Ar$ crystallization
418 ages, but not cooling ages. This relationship can potentially be used to date low-temperature
419 events such as fluid-assisted biotite neo- or recrystallization, as has been demonstrated for white
420 mica (e.g., Cossette et al., 2015; Kellett et al., 2016, 2017).

421 Rapid metamorphic cycles, and short residence times at peak conditions, as documented
422 in many modern orogens, present challenges for interpreting biotite $^{40}Ar/^{39}Ar$ dates. Without
423 sufficient time to diffuse out of biotite, pre-peak radiogenic Ar may be retained even in 0.1 mm-
424 radius grains that experienced moderate temperatures. For instance, during 1 Myr residence at
425 medium pressures, our models suggest that a 0.1 mm-radius biotite grain would only be fully
426 reset (retain 0% pre-peak Ar) if temperatures were sustained at ≥400°C (Fig. 2d).

427 In the eastern Himalaya, biotite dates from an inverted metamorphic sequence (garnet to
428 kyanite-sillimanite grades; 0.4–0.8 GPa) provide empirical evidence of ^{40}Ar inheritance resulting
429 from short-lived metamorphism at moderate temperatures (Mottram et al., 2015). Biotite grains
430 with 0.25 and 0.5 mm radii were dated from the highest-grade part of the sequence, which was
431 metamorphosed at ≥650°C for ~5 Myr, and yielded narrow age populations indicative of cooling
432 ages. In contrast, biotite grains with equivalent radii were analyzed from lower-grade rocks that
433 experienced peak temperatures of 400–580°C for ≤1 Myr. These grains produced discordant
434 heating spectra and dispersed $^{40}Ar/^{39}Ar$ dates that were both older and younger than those of co-
435 existing muscovite (Mottram et al., 2015). The authors attributed this trend to incomplete re-
436 setting of Ar systematics (^{40}Ar inheritance) resulting from short residence times at low
437 temperatures. In support of this interpretation, our models illustrate that a 0.5 mm-radius biotite
438 grain experiencing peak temperatures at 400°C and pressures of 0.4–0.8 GPa would need to
439 remain at those conditions for >20 Myr to achieve complete loss of pre-peak ^{40}Ar (Fig. 2b). For a
440 temperature of 580°C, the same grain would lose all pre-peak ^{40}Ar if it remained at those
441 conditions for ≥1 Myr (Fig. 2a).

442

443 *4.3.3. Precambrian orogens*

444 The models highlight key factors in interpreting $^{40}Ar/^{39}Ar$ dates in Precambrian orogens,
445 where rocks are known to have resided at lower-, mid- and/or upper-crustal conditions for 10s to
446 100s of Myr, or even Gyr timescales. In Precambrian regions, slow cooling rates of ≤10°C/Myr
447 are typically deduced from comparisons between $^{40}Ar/^{39}Ar$ and U–Pb ages (e.g., Schneider et al.,
448 2007; Rivers, 2008; Willigers et al., 2001; Skipton et al., 2017). Alternatively, it has been
449 proposed that $^{40}Ar/^{39}Ar$ dates in Precambrian rocks may be artificially young due to gradual
450 diffusive Ar loss during long-term crustal residence below the Ar closure temperature window
451 (Dunlap, 2000). As a result, rates of cooling and exhumation in Precambrian orogens may have
452 been faster than current estimations. Our modeled P–T–% retention plots support limited Ar loss
453 during long-term, low-temperature crustal residence of fine-grained biotite. For instance, a 0.1
454 mm-radius biotite grain may lose ~25% of its Ar during 1 Gyr of residence at 200°C and 0.3
455 GPa, and ~70% at 275°C (Fig. 3i). However, models of 0.5 mm-radius biotite that resided at
456 250°C for 500 Myr and 1 Gyr exhibit flat core-to-rim age profiles with Ar loss evident only in
457 the outermost ~50 μm of grain edges (Figs. 5b, 6a). The bulk ages of these models are up to 84
458 Myr younger than the onset of crustal residence at 250°C. Our modeling therefore implies that
459 long-term crustal residence at temperatures below the commonly assumed T_c of ~300°C may
460 produce a bulk $^{40}Ar/^{39}Ar$ date several Myr younger than the timing of cooling through ~300°C.
461 This diffusive Ar loss may be detectable within the grain edge using UV laser $^{40}Ar/^{39}Ar$ spot
462 core-to-rim transects with sufficiently high spatial resolution.

463 UV laser age transects have been compared with DiffArgP models to test cooling rates
464 and low-temperature Ar loss in muscovite from the Paleoproterozoic Trans-Hudson Orogen
465 (Skipton et al., 2017). In that case, core-to-rim age profiles generated by DiffArgP models of 1

466 Gyr isothermal residence at 220°C exhibited minor Ar loss at muscovite grain edges, which
467 coincided with dates of UV laser spots. Due to the 50 μm UV spot size and analytical (and
468 model) uncertainties, this relationship was not definitive, but suggests that gradual Ar loss is
469 plausible during long-term isothermal residence at such low temperatures. Importantly, in that
470 study, DiffArgP models simulating various initial cooling rates (1–10°C/Myr) showed that any
471 slow Ar loss that may have occurred during a subsequent 1 Gyr isothermal period in the crust (at
472 T = 220°C) would have been insufficient to change cooling ages beyond uncertainties, or to
473 erase evidence of early rapid (≥10°C/Myr) cooling. Therefore, the muscovite likely cooled at 1–
474 2.5°C/Myr following peak metamorphism, in line with 'slow' cooling rates determined in other
475 Precambrian orogens (Skipton et al., 2017).

476 UV laser spot intra-grain $^{40}Ar/^{39}Ar$ age maps also revealed evidence of slow cooling in
477 biotite from a ca. 1680 Ma synorogenic monzogranite in the Yavapai orogen in the southwestern
478 United States (Hodges and Bowring, 1995). The authors concluded that core-to-rim age
479 decreases of ~200 Myr (from ca. 1240 to 1040 Ma) over 0.5–0.7 mm grain radii resulted from
480 slow cooling following magmatic crystallization, in agreement with independent geological
481 evidence. They used a closure temperature algorithm (Dodson, 1986) to estimate a cooling rate
482 of 0.5 K/Myr. This estimate is supported by our DiffArgP models: models using a faster cooling
483 rate of 1.5°C/Myr yielded more shallowly sloped core-to-rim age gradients (~100 Myr; Figs. 4e–
484 f, 5e–f, 6c) than that of the Yavapai biotite.

485 In some Proterozoic orogens, faster cooling rates have been interpreted from $^{40}Ar/^{39}Ar$
486 dates that are nearly equivalent to metamorphic U/Pb ages. Mid-crustal blocks in the Grenville
487 orogen appear to have cooled at rates up to 11°C/Myr during late-orogenic extension (Cosca et
488 al., 1995; Rivers, 2008; Schneider et al., 2013). Gravity-driven extensional collapse has been

proposed in the Variscan orogen, based on rapid cooling and exhumation deduced in part from $^{40}Ar/^{39}Ar$ ages (e.g., Steltenpohl et al., 1993). "Old" biotite dates that are similar to U/Pb ages of peak metamorphism, suggesting fast cooling, may be reliable if Ar inheritance can be ruled out. This can be evaluated using our model results, together with the known P–T history: the dated biotite must have resided for sufficient time at temperatures in the 'blue' P–T zones (in Figs. 1–3). Theoretically, such biotite would also exhibit a flat core-to-rim age profile indicating rapid cooling (e.g., age profiles for cooling rates of 10°C/Myr and 30°C/Myr in Figs. 4e–f, 5e–f, 6c). However, such an interpretation assumes no $^{40}Ar_e$ contamination, a completely open grain boundary and no trapping of Ar within grain defects; these assumptions are challenging to quantify (discussed below).

4.4. Effects of extraneous Ar and fast-pathway Ar loss

By showing the ages that would be expected following volume diffusion acting alone, our models can help determine whether a biotite $^{40}Ar/^{39}Ar$ date is likely to represent the timing of cooling at a particular rate or if it could have been produced or reset by other processes.

The effects on $^{40}Ar/^{39}Ar$ dates of crystal defects serving as Ar traps (e.g., Camacho et al. 2012) or Ar-loss pathways (e.g., Lee, 1995; Hodges and Bowring, 1995) cannot be directly tested using DiffArgP models. Instead, P–T–% retention plots (Figs. 1–3) provide theoretical constraints on alternative scenarios: e.g., an anomalously young biotite date may result from late, low-temperature biotite crystallization within the 'red zones', and not necessarily from Ar loss through grain defects. Ultraviolet laser spot analyses are important for investigating possible effects of crystal defects on $^{40}Ar/^{39}Ar$ dates; anomalously young zones within biotite may be attributed to grain defects allowing rapid Ar loss (e.g., Hodges and Bowring, 1995; Skipton et al., 2017).

512 The P–T–% retention plots (Figs. 1–3) can be used to assess the likelihood of retention of
513 inherited Ar: biotite that experienced peak conditions within the red or intermediate P–T zones is
514 at risk for containing pre-thermal peak radiogenic Ar, producing a $^{40}Ar/^{39}Ar$ date that may
515 predate the timing of post-thermal peak cooling through T_c. Conversely, if biotite experienced
516 peak P–T in the blue zone, yet yields a $^{40}Ar/^{39}Ar$ date that is older than that expected from
517 independent data, the biotite may have been contaminated by $^{40}Ar_e$.

518 In some cases, $^{40}Ar_e$ contamination can be identified from step-heating analyses (review in
519 Kelley, 2002). It has been suggested that $^{40}Ar_e$ contamination results in saddle-shaped gas release
520 spectra (Lanphere and Dalrymple, 1976; Harrison and McDougall, 1981; McDougall and
521 Harrison, 1999); the shape arising from the suggested release of ^{40}Ar trapped in fluid or melt
522 inclusions at low temperature and from the breakdown of solid inclusions at high temperature
523 (Kelley, 2002).

524 A linear array of step-heating data on an inverse isochron plot may also show the presence of
525 trapped $^{40}Ar_e$ with a distinct non-atmospheric composition (Heizler and Harrison, 1988).
526 However, identification of a $^{40}Ar_e$ component on an isochron plot may be prevented by scattered
527 data, which results from $^{40}Ar_e$ with an inhomogeneous isotopic ratio (e.g., inclusions; Reddy et
528 al., 1997) or, possibly, clustered data resulting from homogenization with radiogenic Ar
529 produced in situ (at $T > T_c$). Additionally, anomalously old biotite dates are commonly
530 calculated from flat 'plateau' gas release spectra (e.g., Pankhurst et al., 1973; Roddick et al.,
531 1980; Foland, 1983; Sherlock et al., 1999; Skipton et al., 2017). In such cases, there is currently
532 no definitive test for $^{40}Ar_e$ contamination, and DiffArgP modeling does not provide one.

DiffArgP can, however, be used to model diffusion of $^{40}Ar_e$ from the grain boundary network into the grain, and comparisons with intra-grain UV laser age spots can shed light on how/when $^{40}Ar_e$ may have been incorporated. For example, in white mica from the Oman high-pressure terrane, UV laser spot transects revealed Ar enrichment in grain rims (Warren et al., 2011). The authors ran DiffArgP models in which $^{40}Ar_e$ was introduced to the grain boundary network (the 'edge age' in Wheeler, 1996) at different stages along the cooling path. When $^{40}Ar_e$ was introduced in the models at 'low' temperatures (i.e., temperatures approaching T_c), the modeled core-to-rim age profiles exhibited Ar-enriched grain rims with anomalously old bulk ages. This led the authors to conclude that the anomalously old white mica could have incorporated $^{40}Ar_e$ late in the cooling history from grain boundary fluids in a closed system, through diffusion or incorporation during recrystallization (Warren et al., 2011). In a similar case, $^{40}Ar/^{39}Ar$ UV laser transects conducted across biotite grains from the Italian Alps yielded dates that increased from core to rim, ranging from ca. 161 to 514 Ma in individual crystals (Pickles et al., 1997). This age pattern was attributed to diffusion of $^{40}Ar_e$ into the grains at temperatures less than 300°C, as supported by theoretically derived curves for volume diffusion of Ar (Pickles et al., 1997).

Incorporation of $^{40}Ar_e$ at high temperatures ($>T_c$, in blue zones in Figs. 1–3), at which Ar diffusion is highly efficient, would theoretically result in diffusive within-grain homogenization of the $^{40}Ar_e$ with radiogenic ^{40}Ar produced *in situ*. As such, the mica would yield an anomalously old date and a smoothly decreasing core-to-rim age profile; this has been illustrated by DiffArgP models of white mica (Warren et al., 2011). Therefore, biotite that yields an anomalously old date but a smoothly decreasing core-to-rim age profile with no evidence of ^{40}Ar-enrichment at grain rims may still contain $^{40}Ar_e$. In this case, biotite would have had to have incorporated $^{40}Ar_e$ during (or prior to) peak P–T conditions in the blue zones in Figs. 1–3, either via diffusion from

556 ^{40}Ar-enriched metamorphic fluids, or incorporation during crystallisation in the presence of ^{40}Ar-
557 enriched fluids. In contrast, $^{40}Ar_e$ enrichment of rims is likely to have occurred at maximum P–T
558 conditions in the red or intermediate zones, such as via low-temperature diffusion from a ^{40}Ar-
559 enriched grain boundary network in a closed system. Our P–T–% retention plots can thus be used
560 in conjunction with the established P–T history to evaluate scenarios of $^{40}Ar_e$ contamination.

561 Figs. 1i, 2c and 2f compare modeled Ar retention in biotite (this study) and muscovite
562 (Warren et al., 2012a) for grain radii of 0.1, 0.5 and 1 mm with 20 Myr residence. The model
563 data reiterate previously established points: muscovite requires higher temperatures than biotite
564 to achieve diffusional loss of pre-thermal peak Ar and resetting of $^{40}Ar/^{39}Ar$ systematics, and has
565 a higher closure temperature window. Therefore, the $^{40}Ar/^{39}Ar$ cooling age of biotite should be
566 younger than that of muscovite in the same rock, provided both minerals grew during the same
567 metamorphic event within the 'blue' P–T zones modeled for biotite (Figs. 1–3) and muscovite
568 (Figs. 3 and 4 in Warren et al., 2012a). Nonetheless, as discussed above, some paired biotite and
569 muscovite dates defy this theoretical relationship. In such cases, muscovite may have crystallized
570 or recrystallized at low temperatures, following cooling through the biotite closure temperature,
571 i.e., within the 'red' P–T zones. A known P–T history is crucial for interpreting this scenario,
572 together with petrographical evidence of late white mica growth/recrystallization. Mica
573 chemistry can also be used to elucidate recrystallized, compositionally distinct muscovite rims
574 (e.g., Cossette et al., 2015). Still, muscovite with no apparent evidence of low-temperature ($<T_c$)
575 growth, compositional zoning or recrystallization has been shown to yield dates younger than
576 those of co-existing biotite in some cases (e.g., Mottram et al., 2015; Skipton et al., 2017). Due
577 to the higher solubility of Ar in biotite than muscovite, biotite may preferentially incorporate
578 $^{40}Ar_e$ (Roddick et al., 1980; Dahl, 1996; review in Kelley, 2002). Anomalously old biotite dates

may result from planar defects in the crystal acting as Ar traps (Camacho et al., 2012). In cases where biotite yields an older $^{40}Ar/^{39}Ar$ date than co-existing muscovite, obtaining UV laser spot transects on both minerals would inform considerations of $^{40}Ar_e$, particularly if localized ^{40}Ar-enriched zones were revealed. Notably, there are currently few intra-grain age data for biotite (Hodges and Bowring, 1995; Pickles et al., 1997) or for co-existing muscovite, which might otherwise be used to further constrain this discussion.

5. Conclusions

The models presented here provide numerical and visual illustration of the percentage of Ar that should theoretically be retained in metamorphic biotite with a variety of grain radii (0.1 to 5 mm) residing for various periods (1 Myr to 1 Gyr) over a range of P–T conditions (Figs. 1–3), given the most reliable currently-available diffusion parameters. The models also demonstrate the effects of different crustal residence temperatures (250–450°C) and durations (1 Myr to 1 Gyr), and of various subsequent cooling rates (1.5–30°C/Myr), on the $^{40}Ar/^{39}Ar$ age and core-to-rim age profile of biotite (Figs. 4–6). Consequently, the models are effective for interpreting metamorphic biotite $^{40}Ar/^{39}Ar$ dates and corresponding cooling/exhumation histories in modern and ancient orogens. As they represent a baseline for %Ar retention, $^{40}Ar/^{39}Ar$ ages and intra-grain age profiles of biotite that are expected from volume diffusion acting alone, the models are also useful for evaluating the likelihood of extraneous ^{40}Ar contamination and non-diffusional ^{40}Ar loss.

The models presented here demonstrate the importance of interpreting $^{40}Ar/^{39}Ar$ ages within an established P–T–t framework: the dated crystal must have attained peak P–T conditions within the ‘blue’ zones (Figs. 1–3) in order to yield a cooling age. Petrographic analyses, mineral

chemical maps and an understanding of the P–T evolution are also key to assessing whether mica recrystallization or dissolution may have reset Ar systematics. A biotite $^{40}Ar/^{39}Ar$ age should be supplemented by a thermochronological age (e.g., muscovite or hornblende $^{40}Ar/^{39}Ar$) from the same rock when possible to provide additional context for the cooling/exhumation history, especially in conjunction with P–T–% retention plots for biotite (this study) and muscovite (Warren et al., 2012a). Paired biotite–muscovite ages may also provide insights into $^{40}Ar_e$ contamination.

The modeled core-to-rim age profiles for biotite presented here strongly support incorporation of the UV laser spot technique into $^{40}Ar/^{39}Ar$ thermochronological studies. Intra-grain age maps have the potential to yield a wealth of information, including diffusional core-to-rim age profiles from which cooling histories can be interpreted, particularly when compared with diffusion models, as demonstrated in previous studies. Ultraviolet laser age maps also enable assessment of: $^{40}Ar_e$; inherited ^{40}Ar; ^{40}Ar loss via fast-diffusion pathways (anomalously young ages in grain centre); and, possibly, low-temperature (<300°C) diffusional Ar loss from grain rims during long-term crustal residence. The ideal size and distribution of UV laser spots (or rasters) depends on several factors, including the analytical set-up and the age of the grain. As shown in earlier studies, UV laser measurements should have the highest possible analytical precision and spatial resolution in a core-to-rim direction to elucidate the intra-grain ^{40}Ar distribution, and to evaluate the best-fit between measured and modeled core-to-rim age profiles.

Cooling/exhumation histories, as classically interpreted from $^{40}Ar/^{39}Ar$ data, must be grounded in theoretical diffusional behaviour, here quantified by DiffArgP modeled bulk ages and core-to-rim age profiles. The temperature, pressure, time and grain-size parameters used in our models correspond to many geological scenarios, and the models can therefore be compared

625 with $^{40}Ar/^{39}Ar$ biotite date to inform interpretations of cooling/exhumation. For geological
626 parameters beyond those modeled here, we recommend numerical diffusion modeling of
627 proposed cooling histories for comparisons with $^{40}Ar/^{39}Ar$ results.

628 The models presented here contain several sources of uncertainty. They are therefore best
629 used in conjunction with $^{40}Ar/^{39}Ar$ biotite data to provide approximate P–T–t constraints on
630 interpreted cooling/exhumation histories or to highlight alternative scenarios, rather than to
631 provide a single 'answer'. Further research to improve constraints on Ar behaviour in biotite will
632 increase confidence in the interpretation of biotite $^{40}Ar/^{39}Ar$ dates as relating to either geological
633 phenomena linked to time, or contamination. In particular, new UV laser $^{40}Ar/^{39}Ar$ spot maps of
634 biotite from various metamorphic regions would provide a more complete library of intra-grain
635 Ar distributions in biotite for comparison with diffusion models, and are an important step
636 toward developing methodology for identifying and quantifying $^{40}Ar_e$ and Ar trapped or lost via
637 grain defects in biotite.

638 **Acknowledgements**

639 DRS acknowledges support from the Alice Wilson Postdoctoral Fellowship, Geological Survey
640 of Canada. Andrew Smye, Dawn Kellett and an anonymous reviewer are thanked for helpful and
641 constructive reviews, which improved the quality of this manuscript. Natural Resources Canada
642 contribution number 20180099.

643 **References**

644 Berger, G.W., 1975. $^{40}Ar/^{39}Ar$ step heating of thermally over-printed biotites, hornblendes, and
645 potassium feldspars from Eldora, Colorado. Earth and Planetary Science Letters 26, 387–
646 408.

Brewer, M.S., 1969. Excess radiogenic argon in metamorphic micas from the Eastern Alps, Austria. Earth and Planetary Science Letters 6, 321–331.

Camacho, A., Lee, J.K.W., Fitz Gerald, J.D., Zhao, J., Abdu, Y.A., Jenkins, D.M., Hawthorne, F.C., Kyser, T.K., Creaser, R.A., Armstrong, R., Heaman, L.W., 2012. Planar defects as Ar traps in trioctahedral micas: A mechanism for increased Ar retentivity in phlogopite. Earth and Planetary Science Letters 341–344, 255–267.

Cosca, M.A., Sutter, J.F., Essene, E.J., 1991. Cooling and inferred uplift/erosion history of the Grenville Orogen, Ontario: constraints from $^{40}Ar/^{39}Ar$ thermochronology. Tectonics 10 (5), 959–977.

Cosca, M.A., Essene, E.J., Mezger, K., van der Pluijm, B.A., 1995. Constraints on the duration of tectonic processes: Protracted extension and deep-crustal rotation in the Grenville orogen. Geology 23 (4), 361–364.

Cossette, E., Schneider, D.A., Warren, C.J., Grasemann, B., 2015. Lithological, rheological, and fluid infiltration control on $^{40}Ar/^{39}Ar$ ages in polydeformed rocks from the West Cycladic detachment system, Greece. Lithosphere 7 (2), 189–205.

Dahl, P.S., 1996. The crystal-chemical basis for Ar retention in micas: inferences from interlayer partitioning and implications for geochronology. Contributions to Mineralogy and Petrology 123, 22–39.

Dallmeyer, R.D., Rivers, T., 1983. Recognition of extraneous argon components through incremental-release $^{40}Ar/^{39}Ar$ analysis of biotite and hornblende across the Grenvillian metamorphic gradient in southwestern Labrador. Geochimica et Cosmochimica Acta 47, 413–428.

669 de Jong, K., Wijbrans, J.R., Féraud, G., 1992. Repeated thermal resetting of phengites in the
670 Mulhacen Complex (Betic Zone, southeastern Spain) shown by $^{40}Ar/^{39}Ar$ step heating
671 and single grain laser probe dating. Earth and Planetary Science Letters 110, 173-191.

672 Dodson, M.H., 1973. Closure temperature in cooling geochronological and petrological systems.
673 Contributions to Mineralogy and Petrology 40, 259–274.

674 Dodson, M.H., 1986. Closure profiles in cooling systems. Materials Science Forum 7, 145–154.

675 Dunlap, W.J., 2000. Nature's diffusion experiment: The cooling-rate cooling-age correlation.
676 Geology 28 (2), 139–142.

677 Foland, K.A., 1983. $^{40}Ar/^{39}Ar$ incremental heating plateaus for biotites with excess argon.
678 Isotope Geoscience 1(1), 3–21.

679 Forster, M.A., Lister, G.S., 2014. $^{40}Ar/^{39}Ar$ geochronology and the diffusion of ^{39}Ar in phengite-
680 muscovite intergrowths during step-heating experiments in vacuo. In: Jourdan, F., Mark,
681 D.F., Verati, C. (eds) 2014. Advances in $^{40}Ar/^{39}Ar$ Dating: from Archeology to Planetary
682 Sciences. Geological Society, London, Special Publications 378, 117–135.

683 Gaber, L.J., Foland, K.A., Corbató, C.E., 1988. On the significance of argon release from biotite
684 and amphibole during $^{40}Ar/^{39}Ar$ vacuum heating. Geochimica et Cosmochimica Acta 52,
685 2457–2465.

686 Giletti, B.J., 1974. Studies in diffusion I. Argon in phlogopite mica. In: Geochemical Transport
687 and Kinetics, Carnegie Institute of Washington Publication, 107–115.

688 Giletti, B.J., Tullis, J., 1977. Studies in diffusion IV: Pressure dependence of Ar diffusion in
689 phlogopite mica. Earth and Planetary Science Letters 35, 180–183.

690 Grove, M., 1993. Thermal histories of Southern California basement terranes. Ph.D. Thesis.
691 University of California, Los Angeles, 419 pp.
692 Grove, M., Harrison, T.M., 1996. ^{40}Ar* diffusion in Fe-rich biotite. American Mineralogist 81,
693 940–951.
694 Hanson, G.N., Simmons, K.R., Bence, A.E., 1975. ^{40}Ar/^{39}Ar spectrum ages for biotite,
695 hornblende and muscovite in a contact metamorphic zone. Geochimica et Cosmochimica
696 Acta 39, 1269–1277.
697 Harrison, T.M., Duncan, I., McDougall, I., 1985. Diffusion of ^{40}Ar in biotite: Temperature,
698 pressure and compositional effects. Geochimica et Cosmochimica Acta 49, 2461–2468.
699 Harrison, T.M., Célérier, J., Aikman, A.B., Hermann, J., Heizler, M.T., 2009. Diffusion of ^{40}Ar
700 in muscovite. Geochimica et Cosmochimica Acta 73, 1039–1051.
701 Harrison, T.M., McDougall, I., 1981. Excess ^{40}Ar in metamorphic rocks from Broken Hill, New
702 South Wales: implications for ^{40}Ar/^{39}Ar age spectra and the thermal history of the region.
703 Earth and Planetary Science Letters 55, 123–149.
704 Heizler, M.T., Harrison, T.M., 1988. Multiple trapped argon isotope components revealed by
705 ^{40}Ar/^{39}Ar isochron analysis. Geochimica Cosmochimica Acta 52, 1295–1303.
706 Hodges, K.V., Bowring, S.A., 1995. ^{40}Ar/^{39}Ar thermochronology of isotopically zoned micas:
707 Insights from the southwestern USA Proterozoic orogeny. Geochimica et Cosmochimica
708 Acta 59 (15), 3205–3220.
709 Kellett, D.A., Warren, C.J., Larson, K.P., Zwingmann, H., van Staal, C.R., Rogers, N., 2016.
710 Influence of deformation and fluids on Ar retention in which mica: Dating the Dover
711 Fault, Newfoundland Appalachians. Lithos 254–255, 1–17.

712 Kellett, D.A., van Staal, C., Wilson, R.A., Rogers, N., 2017. The age of salinic deformation
713 constrained by $^{40}Ar/^{39}Ar$ dating of multiple cleavage domains: Bathurst Supergroup, New
714 Brunswick Appalachians. American Journal of Science 317(3), 338–368.

715 Kelley, S., 2002. Excess argon in K–Ar and Ar–Ar geochronology. Chemical Geology 188, 1–
716 22.

717 Kelley, S.P., Wartho, J.-A., 2000. Rapid kimberlite ascent and the significance of Ar-Ar ages in
718 xenolith phlogopites. Science 289, 609–611.

719 Lanphere, M.A., Dalrymple, G.B., 1976. Identification of excess ^{40}Ar by the $^{40}Ar/^{39}Ar$ age
720 spectrum technique. Earth and Planetary Science Letters 32, 141–148.

721 Lee, J.K.W., 1995. Multipath diffusion in geochronology. Contributions to Mineralogy and
722 Petrology 120, 60–82.

723 Lee, J.-Y., Marti, K., Severinghaus, J.P., Kawamura, K., Yoo, H.-S., Lee, J.B., Kim, J.S., 2006.
724 A redetermination of the isotopic abundances of atmospheric Ar. Geochimica et
725 Cosmochimica Acta 70, 4507–4512.

726 McDougall, I., Harrison, T.M., 1999. Geochronology and Thermochronology by the $^{40}Ar/^{39}Ar$
727 Method. Oxford University Press, New York, New York, 269 pp. (2^{nd} Ed.).

728 Mottram, C.M., Warren, C.J., Halton, A.M., Kelley, S.P., Harris, N.B.W., 2015. Argon
729 behaviour in an inverted Barrovian sequence, Sikkim Himalaya: The consequences of
730 temperature and timescale on $^{40}Ar/^{39}Ar$ mica geochronology. Lithos 238, 37–51.

731 Occhipinti, S.A., Reddy, S.M., 2009. Neoproterozoic reworking of the Palaeoproterozoic
732 Capricorn Orogen of Western Australia and implications for the amalgamation of

733 Rodinia. In: Murphy, J.B., Keppie, J.D., Hynes, A.J. (Eds.) Ancient Orogens and Modern
734 Analogues. Geological Society, London, Special Publications 327, 445–456.
735 Pankhurst, R.J., Moorbath, S., Rex, D.C., Turner, G., 1973. Mineral age patterns in ca. 3700 my
736 old rocks from West Greenland. Earth and Planetary Science Letters 20, 157–170.
737 Pickles, C.S., Kelley, S.P., Reddy, S.M., Wheeler, J., 1997. Determination of high spatial
738 resolution argon isotope variations in metamorphic biotites. Geochimica et
739 Cosmochimica Acta 61 (18), 3809–3833.

740 Powell, R., Holland, T.J.B., 2008. On thermobarometry. Journal of Metamorphic Geology 26,
741 155-179.

742 Reddy, S.M., Kelley, S.P., Magennis, L., 1997. A microstructural and argon laserprobe study of
743 shear zone development at the western margin of the Nanga Parbat – Haramosh Massif,
744 western Himalaya. Contributions to Mineralogy and Petrology 128, 16–29.

745 Rivers, T., 2008. Assembly and preservation of lower, mid, and upper orogenic crust in the
746 Grenville Province – Implications for the evolution of large hot long-duration orogens.
747 Precambrian Research 167, 237–259.

748 Roddick, J.C., Cliff, R.A., Rex, D.C., 1980. The evolution of excess argon in alpine biotites – a
749 ^{40}Ar–^{39}Ar analysis. Earth and Planetary Science Letters 48, 185–208.

750 Scaillet, S., Féraud, G., Lagabrielle, Y., Ballèvre, M., Ruffet, G., 1990. $^{40}Ar/^{39}Ar$ laser-probe
751 dating by step heating and spot fusion of phengites from the Dora Maira nappe of the
752 western Alps, Italy. Geology 18, 741-744.

753 Schneider, D.A., Edwards, M.A., Kidd, W.S.F., Asif Khan, M., Seeber, L., Zeitler, P.K., 1999.
754 Tectonics of Nanga Parbat, western Himalaya: Synkinematic plutonism within doubly
755 vergent shear zones of a crustal-scale pop-up structure. Geology 27 (11), 999–1002.

756 Schneider , D.A., Heizler, M.T., Bickford, M.E., Wortman, G.L., Condie, K.C., Perilli, S., 2007.
757 Timing constraints of orogeny to cratonization: Thermochronology of the
758 Paleoproterozoic Trans-Hudson orogen, Manitoba and Saskatchewan, Canada.
759 Precambrian Research 153, 65–95.

760 Schneider, D.A., Cope, N., Holm, D.K., 2013. Thermochronology of the Mont Laurier terrane,
761 southern Canadian Grenville Province, and its bearing on defining orogenic architecture.
762 Precambrian Research 226, 43–58.

763 Sherlock, S.C., Arnaud, N.O., 1999. Flat plateau and impossible isochrons: apparent 40Ar-39Ar
764 geochronology in a high-pressure terrain. Geochimica et Cosmochimica Acta 63(18),
765 2835–2838.

766 Skipton, D.R., Schneider, D.A., McFarlane, C.R.M., St-Onge, M.R., Jackson, S.E., 2016. Multi-
767 stage zircon and monazite growth revealed by depth profiling and in situ U-Pb
768 geochronology: Resolving the Paleoproterozoic tectonics of the Trans-Hudson Orogen on
769 southeastern Baffin Island, Canada. Precambrian Research 285, 272–298.

770 Skipton, D.R., Schneider, D.A., Kellett, D.A., Joyce, N.L., 2017. Deciphering the
771 Paleoproterozoic cooling history of the northeastern Trans-Hudson Orogen, Baffin Island
772 (Canada), using $^{40}Ar/^{39}Ar$ step-heating and UV laser thermochronology. Lithos 284–285,
773 69–90.

774 Smith, P.E., York, D., Easton, R.M., Özdemir, Ö., Layer, P.W., 1994. A laser $^{40}Ar/^{39}Ar$ study of
775 minerals across the Grenville Front: investigations of reproducible excess Ar patterns.
776 Canadian Journal of Earth Sciences 31 (5), 808–817.
777 Steltenpohl, M.G., Cymerman, Z., Krogh, E.J., Kunk, M.J., 1993. Exhumation of eclogitized
778 continental basement during Variscan lithospheric delamination and gravitational
779 collapse, Sudety Mountains, Poland. Geology 21, 1111–1114.
780 Stübner, K., Warren, C.J., Ratschbacher, L., Sperner, B., Kleeberg, R., Pfänder, J., Grujic, D.,
781 2017. Anomalously old biotite $^{40}Ar/^{39}Ar$ ages in the NW Himalaya. Lithosphere 9 (3),
782 366–383.
783 Uunk, B., Brouwer, F., ter Voode, M., Wijbrans, J., 2018. Understanding phengite argon closure
784 using single grain fusion age distributions in the Cycladic Blueschist Unit on Syros,
785 Greece. Earth and Planetary Science Letters 484, 192-203.
786 Warren, C.J., Sherlock, S.C., Kelley, S.P., 2011. Interpreting high-pressure phengite $^{40}Ar/^{39}Ar$
787 laserprobe ages: an example from Saih Hatat, NE Oman. Contributions to Mineralogy
788 and Petrology 161, 991–1009.
789 Warren, C.J., Hanke, F., Kelley, S.P., 2012a. When can muscovite $^{40}Ar/^{39}Ar$ dating constrain the
790 timing of metamorphic exhumation? Chemical Geology 291, 79–86.
791 Warren, C.J., Kelley, S.P., Sherlock, S.C., McDonald, C.S., 2012b. Metamorphic rocks seek
792 meaningful cooling rate: Interpreting $^{40}Ar/^{39}Ar$ ages in an exhumed ultra-high pressure
793 terrane. Lithos 155, 30–48.
794 Wartho, J.-A., Kelley, S.P., 2003. $^{40}Ar/^{39}Ar$ ages in mantle xenolith phlogopites: determining the
795 ages of multiple lithospheric mantle events and diatreme ascent rates in southern Africa
796 and Malaita, Solomon Islands. Vance, D., Müller, W., Villa, I.M. (eds) Geochronology:

797 Linking the Isotopic Record with Petrology and Textures. Geological Society, London,
798 Special Publications 220, 231–248.
799 Willigers, B.J.A., Krogstad, E.J., Wijbrans, J.R., 2001. Comparison of thermochronometers in a
800 slowly cooled granulite terrain: Nagssugtoqidian Orogen, West Greenland. Journal of
801 Petrology 42 (9), 1729–1749.
802 Wheeler, J., 1996. DiffArg: A program for simulating argon diffusion profiles in minerals.
803 Computers and Geosciences 22(8), 919–929.
804 Van Schmus, W.R., Schneider, D.A., Holm, D.K., Dodson, S., Nelson, B.K., 2007. New insights
805 into the southern margin of the Archean–Proterozoic boundary in the north-central
806 United States based on U–Pb, Sm–Nd, and Ar–Ar geochronology. Precambrian Research
807 157, 80–105.
808 Viete, D.R., Forster, M.A., Lister, G.S., 2011. The nature and origin of the Barrovian
809 metamorphism, Scotland: $^{40}Ar/^{39}Ar$ apparent age patterns and the duration of
810 metamorphism in the biotite zone. Journal of the Geological Society, London 168, 133–
811 146.
812 Villa, I.M., 1994. Multipath Ar transport in K-feldspar deduced from isothermal heating
813 experiments. Earth and Planetary Science Letters 122, 393–401.
814 Villa, I.M., 2010. Disequilibrium textures versus equilibrium modeling: geochronology at the
815 crossroads. In: Spalla, M.I., Marotta, A.M. and Gosso, G. (eds) Advances in
816 Interpretation of Geological Processes: Refinement of Multi-scale Data and Integration in
817 Numerical Modelling. Geological Society, London, Special Publications 332, 1–15.
818 Zimmerman, J.-C., 1972. Water and gas in the main silicate families: Distribution and
819 application to geochronology and petrogenesis. Sciences Terre Memoir 2, 188 pp.

820